



Pseudomonas putida KT2440 metabolism undergoes sequential modifications during exponential growth in a complete medium as compounds are gradually consumed

Journal:	<i>Environmental Microbiology and Environmental Microbiology Reports</i>
Manuscript ID	EMI-2019-0251.R1
Journal:	Environmental Microbiology
Manuscript Type:	EMI - Research article
Date Submitted by the Author:	n/a
Complete List of Authors:	Molina, Lázaro; Centro Nacional de Biotecnología, CSIC, Biotecnología Microbiana La Rosa, Ruggero; Novo Nordisk Foundation Center for Biosustainability, Technical University of Denmark, Nogales, Juan; Centro Nacional de Biotecnología, CSIC, Biotecnología Microbiana Rojo, Fernando; Centro Nacional de Biotecnología, CSIC, Biotecnología Microbiana;
Keywords:	bacteria, metabolic networks, metabolic fluxes, catabolite repression, metabolomics, metabolic models

SCHOLARONE™
Manuscripts

1 **REVISED VERSION**

2

3 ***Pseudomonas putida* KT2440 metabolism undergoes sequential**
4 **modifications during exponential growth in a complete medium as**
5 **compounds are gradually consumed**

6

7

8 **Lázaro Molina¹, Ruggero la Rosa², Juan Nogales¹ and Fernando Rojo^{1,*}**

9

10 ¹ Departamento de Biotecnología Microbiana, Centro Nacional de Biotecnología, CSIC,
11 Madrid, Spain

12 ² Novo Nordisk Foundation Center for Biosustainability, Technical University of Denmark,
13 Kgs. Lyngby, Denmark

14

15 Running head: *P. putida* metabolic fluxes during growth in LB

16

17 ***Correspondence to:** F. Rojo, frojo@cnb.csic.es

18 **E-mail of co-authors:** lmolina@cnb.csic.es; jnogales@cnb.csic.es;

19 rugros@biosustain.dtu.dk

20 **Tel:** (+34) 91 585 45 39; **Fax:** (+34) 91 585 45 06

21

22

23 **Key words:** Metabolism, catabolite repression, metabolic fluxes, metabolomics,
24 metabolic models

25

1 **ABSTRACT**

2

3 *Pseudomonas putida* is a soil bacterium with a versatile and robust metabolism. When
4 confronted with mixtures of carbon sources, it prioritises the utilisation of preferred
5 compounds, optimising metabolism and growth. This response is particularly strong
6 when growing in a complex medium such as LB. This work examines the changes
7 occurring in *P. putida* KT2440 metabolic fluxes while it grows exponentially in LB medium
8 and sequentially consumes the compounds available. Integrating the uptake rates for
9 each compound at three different moments during the exponential growth with the
10 changes observed in the proteome, and with the metabolic fluxes predicted by the
11 *iJN1411* metabolic model for this strain, allowed the metabolic rearrangements that
12 occurred to be determined. The results indicate that the bacterium changes significantly
13 the configuration of its metabolism during the early, mid and late exponential phases of
14 growth. Sugars served as an energy source during the early phase, and later as energy
15 and carbon source. The configuration of the tricarboxylic acids cycle varied during
16 growth, providing no energy in the early phase, and turning to a reductive mode in the
17 mid phase and to an oxidative mode later on. This work highlights the dynamism and
18 flexibility of *P. putida* metabolism.

19

20 **Originality / significance statement**

21 When *Pseudomonas putida* is cultured in a rich medium, carbon sources are used in a
22 hierarchical and sequential manner. This implies important changes in the gene
23 expression programs and in metabolism. Although the molecular details underlying this
24 regulatory response have been investigated for decades, the final effect on the metabolic
25 fluxes is poorly known. This paper shows that, during exponential growth in a rich
26 medium, cells change the configuration of their metabolic fluxes several times, adapting
27 their metabolism to the compounds available without pausing or interrupting growth.
28 Detailed knowledge of the metabolic fluxes that operate under different growth conditions

1 is essential if we are to understand how cells assimilate compounds in the environment,
2 and are to manipulate their metabolism for biotechnological purposes.

3

4

For Peer Review Only

1 Introduction

2 *Pseudomonas putida* KT2440 is a non-pathogenic, Gram-negative soil bacterium with
3 many biotechnological applications (Poblete-Castro *et al.*, 2012). It has been certified as
4 safe strain and approved for release into the environment (Federal-Register, 1982). It is
5 considerably resistant to harsh conditions, has a versatile and robust metabolism, is
6 highly resistant to energetic stress, and has low maintenance demands, all of which
7 render this strain an ideal host organism for bioprocessing and for developing next
8 generation synthetic organisms (Poblete-Castro *et al.*, 2012; Ebert *et al.*, 2011; Nikel *et*
9 *al.*, 2014; Adams, 2016; Belda *et al.*, 2016). Although much is known about *P. putida*
10 KT2440, its large genome (6.18 Mbp; Nelson *et al.*, 2002), its ability to use a wide range
11 of compounds as carbon and energy sources, and its sophisticated regulatory systems,
12 complicate the redirecting of its metabolism towards new functionalities. These
13 properties pose particular challenges when trying to use the organism in bioremediation
14 or biotransformation processes performed in complex growth media containing mixtures
15 of carbon sources, such as waste biological materials.

16 When growing in complex media, pseudomonads use the available resources in a
17 sequential and hierarchical manner, a process that is to a large extent orchestrated by
18 the regulatory process termed catabolite repression (reviewed in Rojo, 2010). In this
19 bacterial group, catabolite repression relies mainly on the Crc and Hfq regulatory
20 proteins, the activities of which are controlled by small RNAs of the CrcZ family
21 (Sonnleitner *et al.*, 2009; Moreno *et al.*, 2012; Moreno *et al.*, 2015; Sonnleitner *et al.*,
22 2018). The influence of this regulatory system is particularly strong in a complex media
23 such as Lysogeny Broth (LB), which is a commonly used medium that allows high growth
24 rates and has been thoroughly used to study the catabolite repression phenomenon. In
25 this medium, the Crc/Hfq regulators influence both the order and the speed of
26 assimilation of compounds available (Moreno *et al.*, 2009; La Rosa *et al.*, 2016).
27 Catabolite repression not only inhibits the assimilation of a given compound until

1 preferred ones have been consumed, it fine-tunes the simultaneous assimilation of
2 multiple compounds (del Castillo and Ramos, 2007; La Rosa *et al.*, 2016). In addition,
3 the different concentrations of available compounds, the efficiency and/or expression of
4 their transport systems, and/or the flux of metabolites through metabolic pathways, might
5 also contribute to define the hierarchy of their assimilation.

6 The sequential assimilation of the compounds in the LB during exponential growth
7 suggests that cells continuously adapt their metabolism as preferred compounds are
8 consumed and new ones start to be used. However, how *P. putida* gradually reorganizes
9 its metabolic fluxes while growing exponentially in a rich medium such as LB has not
10 been analysed in detail. To gain insight into this issue, the assimilation rates of LB
11 components were determined during early, mid and late exponential growth. The data
12 obtained were used to constrain the *i*JN1411 metabolic model for *P. putida* KT2440, and
13 build a series of condition-specific models to provide the most probable flux distribution
14 at each time point. The proteome of the cells at these same time points was analysed to
15 help validating the fluxes predicted. Integrating these three approaches allowed
16 identifying which metabolic pathways were used as cells consumed the different
17 compounds in the medium. The results showed that the *P. putida* metabolic fluxes
18 changed several times during growth, allowing the cells to constantly adapt to changing
19 carbon and energy supplies without the need to stop growth to reprogram metabolic
20 networks, as it occurs in other situations that give rise to a diauxic growth.

21 An interesting finding of this analysis is that the sugars present in the medium were
22 consumed differently during the early, mid and late exponential phases of growth.
23 *Pseudomonas putida* KT2440 can use glucose, fructose and mannose as a carbon
24 source, but is not known to use polysaccharides (Sawyer *et al.*, 1977; Puchalka *et al.*,
25 2008; Dvorak and de Lorenzo, 2018). Glucose assimilation occurs through a cycle
26 formed by enzymes of the Entner-Doudoroff, Embden-Meyerhof-Parnas and Pentose
27 Phosphate pathways (del Castillo *et al.*, 2007; 2008; Nickel *et al.*, 2015). Glucose enters
28 the periplasm via the OprB-I/OprB-II porins and may be directly transferred to the

1 cytoplasm through an ABC transport system, or be oxidised to gluconate in the periplasm
2 by the periplasmic glucose dehydrogenase (Gcd). Gluconate can either be transported
3 into the cell or be further oxidised to 2-ketogluconate in the periplasm by the gluconate
4 dehydrogenase (Gad). The electrons detached from glucose or gluconate during
5 oxidation in the periplasm are transferred to the ubiquinones of the cytoplasmic
6 membrane, feeding the electron transport chain (van Schie *et al.*, 1985; Matsushita *et*
7 *al.*, 1979). The cells can thus use glucose as an energy source without processing its
8 carbon skeleton. The directly internalized glucose and 2-ketogluconate converge into 6-
9 phosphogluconate, which is catabolised to pyruvate and glyceraldehyde 3-phosphate
10 (G3P).

11 Earlier analyses have shown that *P. putida* catabolizes the different amino acids
12 from LB in a hierarchical and sequential way (Moreno *et al.*, 2009; La Rosa *et al.*, 2016).
13 Assimilation occurs through diverse pathways that, depending on the amino acid
14 considered, eventually converge into pyruvate, acetyl-CoA or different intermediates of
15 the tricarboxylic acids (TCA) cycle (Moreno *et al.*, 2009, and references therein). The
16 results showed that the metabolic fluxes derived from the assimilation of these amino
17 acids changed along the growth phase. All these findings highlight the flexibility and
18 dynamism of *P. putida* metabolism.

19

20 **Results**

21

22 *Composition of fresh LB*

23 As a preliminary step, the composition of the fresh LB used in this work was determined;
24 the results are indicated in Table S1 (column labelled "Initial"). This medium is made
25 from tryptone, i.e., a tryptic hydrolysate of casein that provides amino acids and peptides,
26 and yeast extract, which contains sugars, amino acids, peptides, organic acids,
27 (poly)nucleotides, vitamins and micronutrients. The amino acids in LB can, therefore,
28 either be free or form peptides of diverse length. Earlier analyses (La Rosa *et al.*, 2016)

1 of the composition of LB showed free amino acids to be present at a total concentration
2 of 26.8 mM, but those forming part of polypeptides were not detected by the technique
3 used. In the present study, acid hydrolysis of the polypeptides of LB showed the total
4 amino acid concentration to be 86.7 mM (Table S1). This compares well with the 99 mM
5 reported by other authors (Sezonov *et al.*, 2007). Fig. S1 shows the concentrations of
6 free and total amino acids.

7 The LB medium is usually thought to include only scant quantities of carbohydrates
8 (Sezonov *et al.*, 2007; La Rosa *et al.*, 2016). However, this idea derives from studies that
9 used methods able to detect free sugars only, but not polysaccharides. The
10 carbohydrates in LB derive from the yeast extract, which is a concentrate of the water-
11 soluble fraction of autolysed *Saccharomyces cerevisiae* cells. The most abundant
12 carbohydrates in this microorganism are trehalose (a disaccharide of glucose), polymers
13 of glucose (glycogen and β -glucans), and polymers of mannose (mannan) (Aguilar-
14 Uscanga and Francois, 2003; Plata *et al.*, 2013). The precise amount of carbohydrates
15 in LB can vary according to the supplier used. In the present work, the total glucose
16 content (free glucose plus that forming part of polysaccharides) was determined after an
17 acid hydrolysis of the polysaccharides and found to be 14.6 mM (in terms of glucose
18 monomers; Table S1). Most glucose must be forming part of polysaccharides, since free
19 glucose in LB is present at 0.3 mM (La Rosa *et al.*, 2016). *Pseudomonas putida* is unable
20 to use polymers of mannose as a carbon source (see below), therefore the concentration
21 of this polysaccharide was not determined. Low molecular weight organic acids and
22 (poly)nucleotides were also found in the LB used, although at smaller concentrations
23 (Table S1).

24

25 *Consumption of the compounds present in LB*

26 *Pseudomonas putida* KT2440 was inoculated into LB at a turbidity (A_{600}) of 0.05, and the
27 composition of the medium analysed when the cells were in the initial stage of
28 exponential growth (A_{600} of 0.2, after 2 h of growth), in mid exponential growth (A_{600} of

1 0.6, after 3 h of growth), and at the end of exponential growth (i.e., when cells were still
2 actively growing but the growth rate had started to decline; A_{600} of 2, after 7 h of growth;
3 Fig. 1A). The results showed that cells began growth by consuming acetate, succinate,
4 formate, sugars and certain amino acids, mainly glutamine/glutamate (Table S1 and Fig.
5 1-B,C; see also Fig. 2). Succinate, acetate, malate and formate were present at low
6 concentrations and disappeared quickly, as previously reported (La Rosa *et al.*, 2016).
7 Although *P. putida* KT2440 is not known to assimilate the polysaccharides present in LB,
8 the concentration of glucose-polysaccharides decreased by 2 mM during the early
9 exponential phase (labelled as “total glucose” in Table S1; see also Fig. 1C). The
10 disappearance of the sugars during the first 2 hours of growth was paralleled by an
11 increase in the concentration of 2-ketogluconate in the medium up to 2.6 mM (Fig. 1D);
12 this compound was undetectable in the fresh LB at the start of growth. Since *P. putida*
13 oxidises glucose to 2-ketogluconate in the periplasm, which can be released to the
14 medium, the finding of 2.6 mM 2-ketogluconate expelled into the medium after 2 h of
15 growth is strong evidence that the cells were oxidising glucose from the LB but were not
16 catabolising it in the cytoplasm. By mid exponential phase (3 h of growth), the
17 concentration of glucose polysaccharides was reduced to almost half the initial, and
18 further fell during the late exponential phase (Fig. 1C). This was not paralleled by an
19 accumulation of 2-ketogluconate in the medium, which suggests that glucose and 2-
20 ketogluconate were now being metabolised in the cytoplasm.

21 Amino acids were used in a sequential and hierarchical manner. Early exponential
22 growth was characterized by the significant consumption of glutamate/glutamine, lysine,
23 leucine, alanine, aspartate/asparagine, valine, isoleucine, proline, phenylalanine,
24 threonine and serine, the consumption rate being highest for glutamate/glutamine (Table
25 S1). The pattern changed during mid exponential growth when the consumption of many
26 of these amino acids decreased significantly (glutamate/glutamine, leucine,
27 aspartate/asparagine, valine, proline and threonine), or even ceased completely (lysine,
28 alanine, isoleucine and phenylalanine). During this period, however, the consumption of

1 serine and methionine increased. The late exponential phase showed a different pattern
2 again: the consumption of glutamate/glutamine, arginine, leucine, alanine and isoleucine
3 increased once more, and low consumptions of glycine and histidine were detected. This
4 is in general agreement with earlier work showing that, during the first 2-3 h of growth in
5 LB, *P. putida* consumes asparagine, aspartate, serine, proline and glutamate/glutamine,
6 while the assimilation of alanine, arginine, glycine, leucine and isoleucine is delayed until
7 after 4-6 h of culture, the remaining amino acids being used only when cells are in the
8 stationary phase (La Rosa *et al.*, 2016). However, these sets of results should be
9 compared with care, since this earlier work focused on the consumption of free amino
10 acids only; in the present work the consumption of both free amino acids and those
11 present as peptides was measured. The amino acids consumed most strongly
12 throughout the growth period examined were glutamate/glutamine,
13 aspartate/asparagine, arginine and serine (Table S1).

14 Finally, the ammonium concentration in the medium slowly increased over growth,
15 a likely consequence of the assimilation of amino acids. The pH of the medium showed
16 a small increase during the first 2 h of growth and raised from 6.8 to 7.6 during the mid
17 to late exponential phase (Table S1). This is consistent with the preferential use of sugars
18 and organic acids during the first 3 h of growth, and a switch to amino acids thereafter.

19

20 *Modelling the metabolic fluxes at different moments of exponential growth*

21 To understand, in terms of flux distribution, the mechanistic meaning of the nutrient
22 consumption profiles observed experimentally during the early, mid and late exponential
23 phases of growth, we took advantage of the latest genome-scale metabolic model
24 available for *P. putida* KT2440, named *iJN1411*. This model accounts for 2826 metabolic
25 and transport reactions and 1411 genes, and offers a solid representation of *P. putida*
26 metabolism (Nogales *et al.*, 2008; 2017). Condition-specific models corresponding to the
27 metabolic status of the early, mid and late exponential phases were constructed using

1 the experimentally acquired data for the consumption or secretion of metabolites
2 indicated in Table S1. The solution space for each model was examined by flux-balance
3 analysis by maximizing growth rate as the objective function. The subsequent
4 comparison of fluxes distribution between the different condition-specific models allowed
5 the identification of the metabolic shifts that occur throughout the three *P. putida* growth
6 periods analysed. The growth rates (μ) predicted by the model for each time point fitted
7 well with those experimentally determined, with a Kendall's rank correlation coefficient
8 of 0.90 (Fig. 1E). Since any deviation between the *in vivo* and *in silico* growth rates
9 indicates the experimental data to be incomplete, these results strongly support the
10 correct capture of the uptake rates for the nutrients being assimilated *in vivo*, and bear
11 witness to the accuracy of the condition-specific models constructed.

12 The proteome of cells collected at early, mid and late exponential phase were
13 analysed and compared to each other to confirm that the changes in the predicted
14 metabolic fluxes agreed with the increase or reduction in the proteins involved in the
15 corresponding metabolic pathways. More than 1782 proteins were detected, of which
16 between 10.6% and 31.2% changed in abundance during the different phases (Fig. 3A).
17 A visual representation of the changes observed (Fig. 3B) shows that the proteome
18 undergoes substantial change during growth. Of note, when comparing the mid
19 exponential phase with the early phase, most of the differentially expressed proteins
20 were down-regulated. The opposite was observed during the late exponential phase,
21 since most of the differentially expressed proteins relative to the previous phases were
22 up-regulated. The configuration of the metabolic fluxes at each growth phase deduced
23 from these complementary approaches is described below.

24

25 *Configuration of metabolism during the early exponential phase*

26 Feeding the *iJN1411* metabolic model with the nutrients exchange rates experimentally
27 determined during the early exponential phase, indicated in Table S1, allowed an
28 accurate prediction of the metabolic fluxes driving growth during this period. Metabolism

1 at this stage was characterized by the strong oxidation of glucose polymers such as
2 glycogen, maltodextrin (obtained by the partial hydrolysis of glycogen), or β -glucans.
3 *Pseudomonas putida* is not able to use glucose polymers or mannose polymers when
4 provided as the sole carbon source (Dvorak and de Lorenzo, 2018). In fact, the present
5 work confirmed that strain KT2440 cannot grow on starch, cellobiose, maltodextrin, or
6 yeast mannan alone. However, adding a limiting amount of glutamate (5 mM) allowed
7 for robust growth in the presence of starch, cellobiose or maltodextrin (but not mannan),
8 growth that was much faster than that achieved with glutamate alone (Fig. S2). This
9 suggests that strain KT2440 can somehow profit from these glucose polymers if
10 supplemented with an additional carbon and energy source. However, it would not profit
11 from mannose polysaccharides.

12 Glucose (free monomers plus that forming polymers) was present in the fresh LB
13 at 14.62 mM (Table S1). During the early exponential growth, the model-based
14 predictions evidenced that glucose was not transported to the cytoplasm, but was rather
15 oxidised in the periplasm to 2-ketogluconate via gluconate and subsequently excreted
16 to the medium together with a small quantity of gluconate (Figs. 4 and S3A). The
17 oxidation of glucose to 2-ketogluconate, which is coupled to the reduction of the
18 membrane quinones, would render large amounts of reduced quinones to feed the
19 respiratory chain. In support of this, the proteins involved in the uptake and initial
20 oxidation of glucose in the periplasm were detected in the proteome of cells during the
21 early exponential phase of growth, and the concentrations of 2-ketogluconate and
22 gluconate in the growth medium increased after 2 h of growth, confirming that the
23 expulsion of these compounds was indeed taking place (Table S1 and Fig. 1D).

24 The tricarboxylic acids cycle (TCA) in this early phase of growth should rely on the
25 influx of organic acids that are intermediates of this cycle, e.g., citrate, malate and
26 succinate, plus amino acids that are ultimately converted into cycle intermediates, i.e.,
27 arginine (renders succinate), glutamate (renders α -ketoglutarate), or ornithine (renders
28 fumarate) (Figs. 4, 5 and S3). The model predicted that, during this early phase, the TCA

1 cycle ought to operate under an anaplerotic configuration driven by the glyoxylate shunt
2 exclusively, the α -ketoglutarate dehydrogenase complex being inactive (Figs. 4 and S3).
3 As a consequence, a large flux from TCA to G3P was predicted following anaplerotic
4 pathways via oxaloacetate. Ultimately, the G3P produced would be funnelled to glucose
5 6-phosphate (G6P) via gluconeogenesis. Consistently, most of the enzymes required for
6 these reactions were detected in the proteome. These metabolite fluxes towards G6P
7 indicate cells to be operating in a gluconeogenic configuration, which is consistent with
8 the idea that all glucose consumed is oxidised in the periplasm but does not enter the
9 cell during early exponential growth. The model further predicted that the G6P generated
10 would be used to synthesise polysaccharides.

11 Under this scenario, model-based predictions suggested a potential metabolic
12 overflow towards pyruvate. In fact, a large flux from oxaloacetate to pyruvate was
13 predicted via the action of the Prp proteins belonging to methyl-citrate cycle. In addition,
14 pyruvate would also be produced by the transamination of alanine. Around two thirds of
15 this pyruvate would be transformed into acetyl-CoA, and the rest released to the medium
16 either directly or after conversion to lactate (Fig. S3A). In support of this flux
17 configuration, the Prp proteins were detected in the proteome of cells in the early growth
18 phase (Fig. S3A), while the secretion of pyruvate and lactate was experimentally
19 confirmed (Table S1).

20 The model predicted as well an intense flux through amino acid metabolism
21 pathways, which were responsible for providing nitrogenous building blocks for protein
22 and nucleotide biosynthesis. This scenario was largely supported by the anaplerotic
23 configuration of TCA described above. For instance, glutamate/glutamine showed the
24 highest rate of uptake of all the amino acids analysed during the early exponential growth
25 (Table S1). The flux model predicted that glutamine would be transformed into glutamate
26 in the periplasm by the glutaminase-asparaginase (AnsB), which would be internalised
27 and used as a source of α -ketoglutarate, glutamine and ornithine (Figs. 5 and S3B).
28 Glutamine would be used in the biosynthesis of asparagine, histidine and nucleotides,

1 while ornithine would be instrumental as an additional source of arginine. Proline would
2 also be transported from the external medium and transformed into glutamate, although
3 the uptake rates would be about a quarter that of glutamate.

4 The predicted fluxes highlighted an important role for aspartate and asparagine in
5 nitrogen/carbon metabolism during early exponential growth. The uptake rates
6 measured for these amino acids during this phase were a third that of glutamate, but still
7 important (Table S1, Fig. S3B). The model predicted that asparagine would be
8 transformed into aspartate in the periplasm by the AnsB enzyme, and therefore enter the
9 cell as aspartate, which participates in the metabolism of methionine, arginine, fumarate,
10 oxaloacetate and nucleotides. Leucine and lysine were consumed at detectable rates.
11 Alanine, isoleucine and valine were predicted to be catabolised to pyruvate and
12 succinate. Lysine, instead, would be transformed into glutarate, and then released to the
13 medium. The uptake rates for serine, threonine, phenylalanine, arginine and proline were
14 about an eighth to a sixth that of glutamate (Table S1). Fig. S3B shows the fate of each
15 amino acid. Overall, the model predicted that ammonium generated from the metabolism
16 of these amino acids would be used in part to form carbamate (involved in the generation
17 of nucleotides and arginine), the rest being released into the medium. This expulsion
18 was experimentally confirmed (Table S1). The carbon flux prediction also highlighted the
19 use of betaine and threonine as sources of glycine during early exponential growth. This
20 glycine would be further degraded to render ammonium, CO₂ and reducing equivalents
21 through the glycine-cleavage systems (Fig. S3B). Therefore, glycine was predicted to be
22 used as an efficient energy source, but not as a carbon source (Fig. S3B).

23 Overall, nutrients exchange, proteomic analysis and flux prediction during early
24 exponential growth phase suggested that sugars were used as the main energy source
25 via periplasmic oxidation, relegating TCA to a simple anaplerotic assistance. On the
26 contrary, the intense metabolism of amino acids observed was responsible for providing
27 nitrogenous building blocks rather than energy.

1 Finally, the model-based predictions also suggested that, during early exponential
2 growth, polyhydroxyalkanoates (PHAs) would be both synthesised and degraded, the
3 total flux being positive for synthesis. This would require the use of various compounds
4 from the medium catabolized via acetyl-CoA and known to be good precursors of PHA
5 such as acetate, fatty acids, and branched chain amino acids (Fig. 4 and S3A). This
6 agrees with previous reports showing that, in strain KT2440, PHAs are constantly
7 synthesised and degraded even under balanced carbon/nitrogen conditions in order to
8 adapt the carbon flow and reducing power to the demand for cellular intermediates
9 (Escapa *et al.*, 2012). The PhaF and Phal proteins, which are associated to the PHA
10 granules, were detected in the cell's proteome (Table S2).

11

12 *Configuration of metabolism during mid exponential phase*

13 The consumption of sugars, which was strong during the early exponential growth,
14 continued during the mid exponential phase (Table S1). However, while in the initial
15 phase the model predicted that all glucose would be oxidised in the periplasm and the
16 resulting compounds (gluconate and 2-ketogluconate) excreted into the medium, during
17 the mid exponential phase only a small fraction of glucose would be oxidised in the
18 periplasm to form gluconate, and most glucose molecules would enter the cell and be
19 converted into G6P. A small part of this G6P would be funnelled to the glycolytic Entner-
20 Doudoroff pathway while the rest would be directed to the synthesis of glucose-
21 polysaccharides (cellulose, alginate or glycogen) (Fig. 4 and S4). In agreement with
22 these predictions, the expressions of the 1,4- α -glucan branching enzyme GlgB and the
23 glycogen phosphorylase GlgP, which are involved in glycogen metabolism, were lower
24 at the mid exponential phase than during the initial phase (Table S2). The expression of
25 the glycogen synthase GlgE, involved in the elongation of α -(1,4)-glucans, did not vary
26 during these two phases of growth. This suggests that cells were synthesizing glycogen
27 during both, but since degradation decreased during the mid exponential phase, a net
28 accumulation of glycogen occurred. The enzymes involved in cellulose biosynthesis

1 were also detected in the proteome, although their expression did not change. Those
2 involved in alginate biosynthesis were not detected.

3 The fluxes through the TCA were predicted to suffer several changes during mid
4 exponential growth. In fact, the TCA configuration would turn from an anaplerotic to an
5 oxidative mode. This change was sustained by an inhibition of the glyoxylate shunt and
6 the activation of the oxidative step catalysed by α -ketoglutarate dehydrogenase.
7 However, the TCA oxidative mode was far from complete as the other two key steps of
8 the oxidative branch, i.e., isocitrate dehydrogenase and aconitase, were predicted to be
9 inactive. As a result, the transformation of citrate into isocitrate would diminish and the
10 citrate accumulated would be released to the medium (Fig. 4; compare Figs. S3A and
11 S4A). Consistently, the metabolism of amino acids (see below), but not the isocitrate
12 dehydrogenase, was predicted to be the main source of α -ketoglutarate while the flux
13 through the TCA reductive branch was significantly lower than in early growth phase due
14 the absence of glyoxylate shunt as source of succinate. In support of this flux
15 configuration, proteomic analyses indicated that the abundance of the glyoxylate-shunt
16 enzymes AceA and GlcB, as well as that of some isoforms of aconitase (AcnA), isocitrate
17 dehydrogenase (Icd) and fumarase (FumC-II), decreased significantly during mid-
18 exponential phase (Fig. S4B and Table S2). The abundance of the remaining isoforms
19 of these same enzymes (AcnB, Idh, FumA, FumC-I) was similar during the early- and
20 mid-exponential phases of growth.

21 Another modification of the TCA cycle was a change in the fate of malate. Rather
22 than follow the TCA cycle to render oxaloacetate via malate dehydrogenase, as it
23 occurred in the early exponential phase, during the mid exponential phase the model
24 predicted the activation of the pyruvate shunt driven by the malic enzyme (Figs. 4, S4A).
25 This would result in an increase in the NADPH levels that could be used to fight the
26 reactive oxygen species (ROS) derived from the increase in oxidative metabolism
27 predicted at this stage.

1 Regarding amino acids metabolism, it is worth noting that the consumption of
2 lysine, alanine, valine, isoleucine, leucine, histidine and arginine decreased strongly
3 when the cells entered the mid exponential phase, while phenylalanine appeared to be
4 released to the medium (Table S1). The cells now consumed glutamate,
5 aspartate/asparagine, threonine, serine, methionine and proline (Table S1; Figs. 1F, 5,
6 S5A). Accordingly, the flux model predicted that *P. putida* KT2440 metabolism would
7 suffer a reorganization in order to synthesize the amino acids now in shorter supply.
8 Proteomic analyses were in general agreement with these predictions and showed that
9 entry into the mid exponential growth was paralleled by a reduction in the abundance of
10 the enzymes corresponding to many - though not all - pathways for the degradation of
11 amino acids (Fig. S5B, green arrows; Table S2). In contrast, a significant increase in the
12 abundance of proteins involved in the methionine and aspartate transport was observed,
13 in agreement with the detected increase in the use of these amino acids. The absence
14 of changes in the abundance of the enzymes involved in the biosynthesis of amino acids,
15 and the reduction in those involved in their degradation, suggests a net flux balance
16 directed towards the biosynthesis of amino acids, just as predicted by the condition-
17 specific model. In agreement with this active anabolism, with the depletion of several
18 metabolites in this stage such as fatty acids, and with the requirement of additional
19 carbon skeletons, model-based predictions suggested cells cease to produce PHAs, with
20 the existing polymer reserves being degraded (Figs. 4 and S4A). Proteomic analyses
21 (Table S2) agreed with this prediction since a reduction was detected in the abundance
22 of the PhaF and Phal proteins associated to the PHA granules. In the same line, the
23 secretion of lactate and pyruvate would cease; in fact, they were recovered from the
24 medium and catabolised (Figs. 4 and S4A; Table S1).

25 Taken together, the analysis of metabolic fluxes in the mid-exponential phase
26 suggested that sugar oxidation in the periplasm was partially replaced by the TCA as the
27 main source of energy. In addition, the progressive depletion of preferred metabolites
28 likely forced cells to adopt a more efficient metabolism of glucose, starting its complete

1 mineralization. Finally, it seems that *P. putida* displayed a metabolite recovery program
2 in this stage to supply the higher demand of carbons skeleton required for anabolism.

3

4 *Configuration of metabolism during the late exponential phase*

5 Seven hours after inoculation, the increase in biomass and in total cell numbers indicated
6 that cells were still actively growing at a rate similar to that observed during the mid
7 exponential phase, although exponential growth was reaching its end (Fig. 1A, E). Most
8 of the changes observed during the transition from the early to the mid exponential
9 phases were now reverted. The use of glucose decreased substantially during the late
10 exponential phase (Table S1 and Fig. 1C). The model predicted that all glucose entering
11 the cell would be transformed into gluconate in the periplasm by the glucose
12 dehydrogenase Gcd, with all gluconate entering the cytoplasm (Figs. 4 and S6A). About
13 90% of this gluconate would be transformed into pyruvate via the Entner–Doudoroff
14 pathway, which would be used to synthesise acetyl-CoA. The remaining 10% would be
15 diverted to the pentose phosphate pathway to form ribulose-5-phosphate, G3P and
16 fructose-6-phosphate. The flux model predicted that the cells would reduce or cease the
17 synthesis of intracellular glucose polymers (Fig. 4). In agreement, the abundance of the
18 glycogen synthase GlgE was found to be reduced, while those of GlgB (1,4- α -glucan
19 branching enzyme) and GlgP (α -1,4 glucan phosphorylase) increased (Table S2). This
20 suggests that, when entering the late exponential phase, cells degrade the
21 polysaccharides accumulated in the previous phase to obtain glucose.

22 In addition, the incipient oxidative mode of TCA adopted during the mid exponential
23 phase became more evident during this late growth phase and the flux model predicted
24 that the cycle would be fully activated (Fig. 4). In agreement with this prediction, many
25 of the cycle enzymes became more abundant during the late exponential phase (Fig.
26 S6B, red arrows, and Table S2). The increase was observed for all isoforms of the
27 enzymes affected with the exception of succinyl-CoA synthetase (SucC and SucD) and
28 succinate dehydrogenase (SdhABCD), which were already abundant during the previous

1 growth phase, and the enzymes that oxidise malate (Mdh remained constant, Mqo-1
2 increased, and Mqo-2 decreased).

3 The flux model predicted an increase in the rate of degradation of fatty acids at this
4 point. In agreement with this, the abundance of several enzymes responsible for the β -
5 oxidation of fatty acids (FadA, FadBA, FadB, the enoyl-CoA hydratase PP_1845, FadE)
6 were found to be increased relative to the previous phase (Fig. S6B and Table S2). The
7 abundance of proteins related to acetate generation (AcsA) and PHA metabolism (BktB,
8 Hbd, PhaC1 and PhaF) also increased (Fig. S6B). All this led to the pool of acetyl-CoA
9 becoming larger and an increase in the synthesis of PHAs, as predicted by the flux
10 model. In agreement with this idea, the abundance of the enzymes involved in the
11 glyoxylate shunt also increased in order to metabolize the acetyl-CoA produced.

12 The metabolism of amino acids also changed when the cells reached the late
13 exponential phase. Proteomic analyses and model predictions suggested the cells to
14 now grow at the expense of amino acids. The uptake of arginine, alanine, leucine,
15 isoleucine, glutamate/glutamine and histidine increased. The transport of glutamate
16 remained active, allowing it to serve as a donor of amine groups for the biosynthesis of
17 other amino acids. Importantly, proteins annotated as oligopeptide transporters
18 increased in abundance, which might allow cells to use serine or proline, the free forms
19 of which would likely have been exhausted during the earlier phase of growth (La Rosa
20 *et al.*, 2016). Other transporters were activated during late exponential growth, such as
21 those for the polyamine putrescine and γ -aminobutyric acid (GABA). The direct
22 determination of GABA showed that it was indeed present in the initial LB at low
23 concentration, but had been largely consumed by this point in growth (Table S1). In
24 contrast, the uptake rates for methionine, aspartate and threonine were experimentally
25 observed to decrease (Table S1 and Fig. 5), as was the abundance of proteins involved
26 in their transport (Fig. S7B). This intense catabolism of amino acids is consistent with
27 the fully oxidative mode of TCA as main source of energy.

1 Finally, it is worth noting that the metabolism of glutathione was activated during
2 late exponential growth. An increase was detected in the abundance of the enzymes
3 involved in its biosynthesis (GshB glutathione synthetase) and degradation (Ggt γ -
4 glutamyltranspeptidase and PepN aminopeptidase) (Fig. S7B and Table S2). This
5 tripeptide reduces oxidised proteins. The abundance of the glutathione reductase Gor,
6 which regenerates oxidised glutathione, also increased, as did that of several enzymes
7 involved in the detoxification of ROS, such as the catalases KatA and KatG, the alkyl-
8 hydroperoxide reductase AhpC, and the peroxidase Tpx. All this suggests that the cells
9 were exposed to oxidative stress during this late phase of growth. The use of the 2,3,5-
10 triphenyl-2H-tetrazolium chloride (TTC) reduction assay showed that the redox state of
11 the cells was low during the early and mid exponential phases, but increased significantly
12 during the late exponential phase (Table S1). This indicates that during the latter phase,
13 the concentration of ROS increases, which fully agrees with the TCA fully operating in
14 an oxidative mode.

15

16 Discussion

17 When preferred compounds are exhausted early during growth in a complete medium
18 such as LB, cells need to adapt their metabolism towards the less preferred compounds
19 that remain. By visualizing the metabolic fluxes at three moments during exponential
20 growth in LB, the present work provides greater insight in this issue by reconstructing
21 the dynamic carbon flux readjustment driving this behaviour. The results, which are
22 summarised in Fig. 6, show for the first time how, when using this medium, *P. putida*
23 completely changes the configuration of its central and peripheral metabolism during
24 exponential growth in response to changing nutrient availability. During growth from the
25 early to the late exponential phase, we monitored a gradual change in (a) the mode of
26 energy generation; (b) the TCA configuration, which changed from anaplerotic to
27 oxidative; (c) the metabolism of sugars, which changed from gluconeogenic to glycolytic;

1 (d) the metabolism of amino acids, which were first used as carbon source and later on
2 as energy source, and (e) the carbon storage metabolism. This gradual change was
3 paralleled by a lineal increase in ROS generation which was retaliated by an increase in
4 NADPH generation. It seems plausible that *P. putida* avoids unnecessary cytoplasmic
5 anabolism and oxidative metabolism while minimizing the production of ROS under
6 nutritionally rich conditions. Depletion of preferred nutrients forced *P. putida* to adopt a
7 more efficient oxidative metabolism which was balanced with a higher NADPH
8 production to minimize potential deleterious effects due the expected increase in ROS.

9 The control of metabolic fluxes in response to the concentration of key metabolites
10 is a complex and poorly known phenomenon that is of vital importance to coordinate
11 microbial metabolism (Chubukov *et al.*, 2014). Cells began growth using organic acids
12 such as acetate and different TCA intermediates (citrate, malate and succinate), and a
13 selected set of amino acids (mostly glutamate/glutamine), as their carbon sources.
14 Sugars (glucose monomers and apparently glucose polymers derived from yeast extract)
15 were also consumed during this early stage, but the proteomic data collected, the flux
16 model, and the detected secretion of 2-ketogluconate, all indicate that these sugars were
17 not used as a carbon source but as a supply of electrons to feed the electron transport
18 chain, i.e., they were used as energy source. The oxidised sugar products were mostly
19 released into the medium. Glucose polymers were present in substantial concentrations.
20 It should be stressed that different sources of yeast extract can include different amounts
21 of sugars, which might influence the metabolic configuration of cells.

22 It is still not clear how cells managed to use glucose polysaccharides. Although *P.*
23 *putida* KT2440 could not grow on starch, cellobiose or maltodextrin alone, robust growth
24 occurred if a limiting amount of glutamate was provided as well (Fig. S2). This suggests
25 that *P. putida* can in fact profit from these sugar polymers. The genome of strain KT2440
26 encodes some enzymes that might be instrumental in depolymerising glucose polymers.
27 These include PP_1403 (BglX), a periplasmic glucohydrolase that catalyses the
28 hydrolysis of glycosidic bonds in β -D-glucans with the release of glucose, and the product

1 of PP_1126, which codes for a periplasmic glycoside hydrolase. Both these enzymes
2 were detected in the cell proteome, although their abundance seemed to change little
3 throughout growth. Cells might secrete other glucanases that escaped the present
4 proteomic analyses.

5 During the early growth phase, the TCA cycle seemed to operate solely via the
6 glyoxylate shunt, a configuration characteristic of situations in which cells grow at the
7 expense of 2- or 3-carbon organic acids, or fatty acids (Fig. 4). This means that isocitrate
8 dehydrogenase and α -ketoglutarate dehydrogenase, which are important providers of
9 NADH, were not active, and most energy (reducing power) was provided by the oxidation
10 of glucose in the periplasmic space, and by oxidation of the glycine produced from
11 threonine and betaine. In *Pseudomonas aeruginosa*, flux distribution between the TCA
12 cycle and the glyoxylate shunt is coordinated through the reciprocal regulation of
13 isocitrate dehydrogenase and isocitrate lyase; low concentrations of oxaloacetate and
14 pyruvate inhibit isocitrate dehydrogenase and activate isocitrate lyase, favouring the
15 glyoxylate shunt and reducing the flow through the TCA (Crousilles *et al.*, 2018). Our
16 results are consistent with oxaloacetate and pyruvate being in short supply during the
17 early growth phase, and suggest that a flux from oxaloacetate towards glucose-6P
18 occurred, the cells being in a gluconeogenic configuration.

19 This metabolic configuration changed as the cells entered the mid exponential
20 phase, with the contribution of organic acids and several amino acids decreasing
21 substantially. Unsurprisingly, the cells turned to glucose to sustain their growth and some
22 glucose and gluconate molecules now entered the cell and were directed either towards
23 the TCA cycle or to the synthesis of polysaccharides. The TCA cycle was also fed via
24 the increased uptake of aspartate and the recycling of compounds excreted in the
25 previous phase, such as pyruvate and 2-ketogluconate. This sudden funnelling of
26 metabolites towards TCA could not be processed properly and a bottleneck appeared
27 resulting in the secretion of citrate. A few hours later, when the cells entered into the late
28 exponential phase of growth, this picture changed again substantially. The use of sugars

1 as a carbon source continued; this was reinforced by the depolymerisation of the
2 polysaccharides accumulated intracellularly in the previous phases. Several amino
3 acids, most notably arginine, were used as a source of TCA intermediates, and the citrate
4 extruded in the previous phase was recovered and processed in the TCA cycle, which
5 now started to function actively in a fully cyclical manner, i.e., in its fully oxidative mode,
6 increasing the supply of NADH. This was paralleled by an increase in the production of
7 ROS and in the elements devoted to fight oxidative stress (glutathione, catalases, etc). The
8 cells used different amino acids in each growth phase, the bias between amino acid
9 synthesis and degradation shifting towards synthesis during the mid exponential phase,
10 and returning towards degradation in the late exponential phase.

11 All the data collected are consistent with the sequential and hierarchical use of the
12 compounds present in LB, and a progressive rearrangement of the cells' metabolism so
13 that the way of obtaining energy and carbon building blocks evolved and adapted to the
14 continuously changing conditions. All these changes occurred without any noticeable
15 interruption in cell growth, although perhaps cells experienced multiple, shifting
16 limitations, as suggested earlier (Wittgens *et al.*, 2011). This might be the result of gene
17 expression being highly optimized, but also of the fact that, despite the hierarchical
18 assimilation of the compounds present, several were used simultaneously at each time
19 point, the exhaustion of one being compensated by the assimilation of alternatives. The
20 overall picture, therefore, is that of a very flexible and well-coordinated metabolism that
21 allows adaptation to the prevailing conditions while maintaining vigorous growth. It is
22 worth stressing that, despite the strong use of sugars through growth, glucose transport
23 and assimilation is known to be under catabolite repression, a process controlled by the
24 Hfq/Crc proteins. Inactivating the gene coding for Crc increased the glucose assimilation
25 rate and the expression of the genes involved in the transport and assimilation of glucose
26 (Moreno *et al.*, 2009; del Castillo and Ramos, 2007; La Rosa *et al.*, 2016). The results
27 presented here show that this repression did not impede the use of glucose (or glucose
28 polymers) as an energy source at the start of growth, although neither glucose nor

1 glucose oxidation products appeared to be used as a carbon source until the second
2 period of the exponential growth. This indicates that the regulation of glucose
3 assimilation is complex.

4 Inactivation of the gene coding for the Crc protein is known to cause an 8-10%
5 reduction in the growth rate of strain KT2440 in LB; its metabolism is destabilised and
6 cell fitness reduced, allowing wild type cells to rapidly out-compete the mutant strain
7 (Moreno *et al.*, 2009; La Rosa *et al.*, 2016). This shows that catabolite repression is
8 involved in the optimisation of metabolism, which helps explain the success of *P. putida*
9 as an opportunistic and cosmopolitan bacterium. A detailed knowledge of the metabolic
10 fluxes that operate under different growth conditions is essential if we are to understand
11 how cells function, and if we are to use their metabolism for desired ends. The present
12 results are a step in this direction.

13

14 **Experimental Procedures**

15 *Bacterial strains and culture media*

16 *P. putida* KT2440 (Franklin *et al.*, 1981) was cultured at 30°C in LB (10 g/L tryptone, 5
17 g/L yeast extract, 10 g/L NaCl). Tryptone and Yeast Extract were obtained from Conda
18 (Spain). The ability of this bacterial strain to use polysaccharides as the carbon source
19 was determined in M9 minimal salts medium (Sambrook and Russell, 2001)
20 supplemented with trace elements (Bauchop and Eldsen, 1960); its final composition
21 was 42.4 mM Na₂HPO₄, 22 mM KH₂PO₄, 8.6 mM NaCl, 18.7 mM NH₄Cl, 25 µM CaCO₃,
22 1.2 µM CoSO₄, 1.3 µM CuSO₄, 42.7 µM FeSO₄, 0.4 µM H₃BO₃, 776 µM HCl, 333 µM
23 MgO, 38.1 µM MnSO₄, 6.25 µM ZnSO₄. The polysaccharides tested were potato starch,
24 cellobiose, maltodextrin and mannan (from *S. cerevisiae*). These were added at 0.25 %
25 (w/v) in the presence or absence of 3 mM glucose or 5 mM glutamate.

26

27 *Determination of chemical compounds in LB during P. putida growth*

1 Twenty ml of fresh LB were inoculated with overnight cultures of the microorganism at a
2 turbidity (A_{600}) of 0.05. The cultures were incubated at 30°C to an A_{600} of 0.2 (early
3 exponential growth), 0.6 (mid exponential growth) or 2 (late exponential growth). At these
4 time points they were centrifuged at 7500 x rpm for 10 min and the supernatants obtained
5 filtered through 0.22 μm pore filters (Millipore-Merck) to eliminate cells. Then, they were
6 frozen at -80°C until analysis. The content of sugars, organic acids and amino acids in
7 these samples was analysed using previously described methods. To determine the total
8 amount of glucose, glucose polysaccharides in the samples were hydrolysed by
9 treatment with 2 M trifluoroacetic acid at 120°C for one hour. Glucose was then detected
10 by HPLC using a 920LC Agilent apparatus equipped with a PL-EDS 2100 Ice detector
11 and an Asahipak NH₂-50 E column (Shodex). The mobile phase was an
12 acetonitrile/water gradient as follows: t=0, 77%; t=10, 77%; t=17, 65%; t=20, 65%;
13 t=20.1, 77%; t=25, 77% (t in min, % refers to acetonitrile concentration); the flow rate
14 was 1.2 ml min⁻¹. Three independent assays were performed.

15 The content of 2-ketogluconate was determined as previously described (Lanning
16 and Cohen, 1951). In brief, 1 ml of 2.5% (w/v, in water) o-phenylenediamine
17 dihydrochloride was mixed with 2 ml of LB or filtered culture supernatants. After heating
18 in boiling water for 30 min, the absorbance of the reaction mixture was measured at 330
19 nm. A standard curve was prepared using different concentrations of 2-ketogluconate.
20 Three independent assays were performed.

21 Gluconate, lactate and fatty acid concentrations were determined using the D-
22 gluconic acid/D-glucono- δ -lactone assay kit (Megazyme), the Lactate Assay Kit (Sigma-
23 Aldrich), and the Free Fatty Acid Quantification Kit (Sigma-Aldrich), respectively.
24 Polynucleotide quantification was performed using the DNA Quantification Kit (Sigma-
25 Aldrich) and the Quant-iT Oligreen ssDNA Kit (Thermo Fisher Scientific). The
26 consumption of individual nucleotides was estimated on the basis of the G+C content of
27 *S. cerevisiae* (38%). The concentrations of α -ketoglutarate, citrate, GABA, isocitrate and

1 malate were determined by HPLC/MS using a 1200L Varian device fitted with an ACE
2 Excel 5 C18-Amide column (250 mm x 4.6 mm). The mobile phase was 0.1% formic acid
3 in water at a flow rate of 0.4 ml/min. Ammonium was quantified using the Ammonia Assay
4 Kit AA0100 (Sigma-Aldrich). Three independent assays were performed in all cases.

5 The total amino acid content of the culture samples (free plus those forming
6 polypeptides) was determined after an acid hydrolysis of the samples for 20 h at 110°C
7 in 6 M HCl, 0.1% phenol and 0.1% thioglycolic acid under reduced pressure in an argon
8 atmosphere. Identification and quantification of the amino acids was performed by
9 Alphalyse (Denmark) with a BioChrom 30 amino acid analyser using ion exchange
10 chromatography, post-column derivatization with ninhydrin, and detection at 570 nm and
11 440 nm. A known amount of the amino acid sarcosine was added as an internal standard
12 control. The 20 common amino acids, except for tryptophan and cysteine, were all
13 determined in duplicate.

14 The redox potential of the cells was measured by collecting them from 1.5 ml of
15 culture and treating them with 2,3,4-triphenyl-2H-tetrazolium chloride as previously
16 described (Defez *et al.*, 2017). pH was measured using a pH-meter. To determine the
17 dry weight of culture samples, 50 ml of culture were centrifuged at 7000 x rpm for 10
18 min. The resulting pellets were dried for 24 h at 60°C and weighed using an analytical
19 balance.

20

21 *Constraint-based analyses of metabolic fluxes*

22 The most recent and complete genome-scale metabolic model of *P. putida* KT2440,
23 *iJN1411*, was used for all metabolic flux estimations (Nogales *et al.*, 2017). *iJN1411*
24 includes 2826 metabolic and transport reactions, 2087 metabolites and 1411 genes, and
25 provides the best available representation of *P. putida* metabolism. The model accounts
26 for a large number of reactions mimicking the exchange with the environment of up to
27 337 different metabolites. *iJN1411* is able to use 220 metabolites as the sole carbon and

1 energy source, as well as 105 metabolites as the sole nitrogen source. In addition,
2 *iJN1411* can account for growth in rich media, such as LB (Nogales *et al.*, 2017). Flux
3 balance analysis (FBA) (Varma and Palsson, 1995, Orth *et al.*, 2010) was used to make
4 growth rate predictions and to determine initial flux distributions. FBA is based on solving
5 linear optimisation problems by maximising or minimising a given objective function \mathbf{Z}
6 subject to a set of constraints. The constraint $\mathbf{S}\cdot\mathbf{v} = \mathbf{0}$ corresponds to a situation of
7 steady-state mass conservation where the change in concentration of the metabolites
8 as a function of time is zero. "S" is an $m \times n$ matrix containing all the stoichiometric
9 coefficients in the model of m metabolites and n reactions, and the vector "v" has n
10 elements that represent the individual flux values for each reaction. These fluxes are
11 additionally constrained by the imposed lower and upper limits (bounds) "vl" and "vu".
12 The output is a flux distribution that maximises or minimises a given objective function.
13 The growth rate was used routinely as the objective function. The output is a flux
14 distribution that maximises or minimises a given objective function - in this case the
15 growth rate. All computational simulations were performed using the COBRA toolbox
16 (Schellenberger *et al.*, 2011) in the MATLAB environment (The MathWorks Inc.). Linear
17 optimization problems were solved using the GNU Linear Programming Kit (GLPK)
18 (<http://www.gnu.org/software/glpk>).

19

20 *Construction of growth-phase condition specific models*

21 To simulate bacterial growth in LB, an initial *in silico* medium was defined based on the
22 composition of LB and the reported gene analysis of strain KT2440 (Oh *et al.*, 2007;
23 Nogales *et al.*, 2017; Molina-Henares *et al.*, 2010). The initial *in silico* LB composition
24 was completed with the metabolites detected in the present analyses (Table S1). Thus,
25 the default growth conditions for LB included the free uptake of those metabolites present
26 in the medium while allowing for the free exchange of CO_2 , H_2O , H^+ , HCO_3^- , Na^+ , NH_4^+ ,
27 Pi , Fe^{2+} and SO_4^{2-} . Constraint-based metabolic models calculate intracellular flux

1 distributions that satisfy three fundamental types of constraints: steady-state mass-
2 balance, reaction reversibility, and flux capacities. For the latter, the flux measured for a
3 given reaction, including nutrient uptake rates, can be imposed on the model,
4 constraining the solution space. The growth-phase specific models were therefore
5 constructed by constraining to experimental values the bounds of the exchange
6 reactions corresponding to the different compounds for which uptake and/or secretion
7 rates could be determined (sugars, organic acids, amino acids, lipids, nucleotides and
8 ammonium) at each time point (Table S1). Specific models reproducing the growth rate
9 and nutrient exchange during early, mid and late exponential growth, could therefore be
10 constructed.

11

12 *Quantitative analysis of proteomes by mass spectrometry (MS) using isobaric tagging*
13 *relative and absolute quantitation (iTRAQ)*

14 Proteomic analyses were performed at the CNB-CSIC proteomics facility (Madrid, Spain;
15 <http://proteo.cnb.csic.es/proteomica/>) using the iTRAQ procedure. Forty, 20 or 10 ml of
16 bacterial suspension obtained from cultures at a turbidity of 0.2, 0.6 or 2.0 respectively
17 were centrifuged for 5 min at 13,000 x g at 4°C. The cell pellets were washed twice in 10
18 ml of 0.1 M PBS buffer (10 mM Na₂HPO₄, 2 mM KH₂PO₄, pH 7.4, 137 mM NaCl, 2.7 mM
19 KCl) and stored at -80°C. These frozen cell pellets were resuspended in 0.5 ml of 0.1 M
20 PBS buffer pH 7 containing a cocktail of protease inhibitors (cComplete™ Mini from
21 Roche) and disrupted by sonication on ice. Cell debris was eliminated by centrifugation
22 at 13,000 x g for 20 min at 4°C. The protein concentration was determined using the
23 Pierce™ BSA Protein Assay Kit (ThermoFisher Scientific). Proteins in the supernatant
24 were precipitated with methanol/chloroform (Wessel and Flugge, 1984) and
25 resuspended in 160 µl of a buffer containing 7 M urea, 2 M thiourea and 100 mM
26 tetraethylammonium bromide. For iTRAQ tagging, 40 µg of proteins from two sample
27 were digested overnight at 37°C with 4 µg of trypsin (Sigma-Aldrich, USA). The resulting

1 peptides were labelled for 2 h with iTRAQ tags (AB Sciex; one tag for each sample, 6-
2 plex procedure). The labelled samples were then mixed and cleaned by passage through
3 a C18 SEP-PAK column. An amount of sample equivalent to a total of 1 μg of labelled
4 peptides was analysed by liquid chromatography/mass spectrometry in an AB Sciex
5 Triple Q-TOF mass spectrometer.

6 Protein identification and the analysis of protein differential expression were
7 performed by Proteobotics S.L. (Madrid, Spain). Briefly, MS/MS spectra were exported
8 to *mgf* format using Peak View v1.2.0.3 and examined, using Mascot Server 2.5.1,
9 OMSSA 2.1.9, X!TANDEM 2013.02.01.1, and Myrimatch 2.2.140 software against a
10 composite target/decoy database built from the 5313 *P. putida* KT2440 sequences held
11 in the Uniprot Knowledgebase (November 2015), together with commonly occurring
12 contaminants. Search engines were configured to match potential peptide candidates
13 with a mass error tolerance of 25 ppm and a fragment ion tolerance of 0.02 Da. Up to
14 two missed tryptic cleavage sites and a maximum isotope error (^{13}C) of 1 were allowed,
15 contemplating fixed methyl-methane-thiosulphonate modification of cysteine and the
16 variable oxidation of methionine, pyroglutamic acid derived from glutamine or glutamic
17 acid at the peptide N-terminus, and the modification of lysine and the N-terminus by
18 Tandem Mass Tags (TMT) 6-plex reagents. Score distribution models were used to
19 compute peptide-spectrum match *p*-values (Ramos-Fernández *et al.*, 2008). Spectra for
20 peptides recovered after filtering with a false discovery rate of ≤ 0.01 were selected for
21 quantitative analysis. Approximately 1% of the signals of the lowest quality were
22 removed. Differential regulation was measured using linear models (López-Serra *et al.*,
23 2014). Statistical significance was measured using *q*-values (FDR). All analyses were
24 conducted using software from Proteobotics. Proteins showing an abundance change of
25 ≥ 1.4 fold (\log_2 fold change of 0.49), and a *q*-value of ≤ 0.05 , were considered differentially
26 expressed (Koul *et al.*, 2014).

27

28

1 **Acknowledgements**

2 We are grateful to L. Yuste for excellent technical assistance. This work was funded by
3 grants BIO2015-66203-P to FR and BIO2014-59528-JIN to JN from Ministerio de
4 Ciencia, Innovación y Universidades, Spain (AEI/FEDER, EU). Authors have no
5 conflicts of interest to declare.

6

For Peer Review Only

1 FIGURE LEGENDS

2

3 **Figure 1. Growth of *P. putida* KT2440 in LB and consumption of different**
4 **compounds. (A)** Increase in turbidity (A_{600}) and in colony forming units (cells/ml) during
5 growth in LB. Consumption of organic acids (**B**), sugars (glucose monomers and
6 polymers) (**C**), amino acids (**F, G**) and (poly) nucleotides (**H**) during growth. (**D**) Release
7 of 2-ketogluconate and gluconate to the medium and consumption of glycerol during
8 growth. (**E**) Growth rate at each time point relative to the previous point (or to the
9 inoculated cells in the case of the first time point); data derived either from the
10 experimentally determined increase in biomass (μ real), or from the increase predicted
11 by the flux model (μ flux model). Error bars indicate the standard deviation of three
12 independent assays. The scale of the time axis is not the same in all panels.

13

14 **Figure 2. Hierarchical clustering of the exo-metabolomic profiles of *P. putida*.** The
15 normalised concentrations (range scaling) of each metabolite identified in the non-
16 inoculated medium (t0), or in medium samples collected at the early (t1), mid (t2) and
17 late (t3) exponential phases of growth (data derived from Table S1), were clustered
18 according to Euclidean distances using the Ward clustering algorithm (Ward Jr, 1963)
19 and employing JMP software v.13.2. The highest normalised concentration for each
20 compound is indicated in red colour, while the lowest concentration is in blue.

21

22 **Figure 3. Comparison of the proteome of cells collected at early, mid and late**
23 **exponential growth. (A)** Number of proteins detected and compared under each
24 condition, and those differentially expressed (q -value <0.05 , fold-change >1.4 , as
25 recommended (Koul *et al.*, 2014)). (**B**) Volcano plots of the proteins showing increased
26 or decreased abundance during early, mid and late exponential growth. Differentially
27 expressed proteins are listed in **Table S2** (Supplementary Material).

28

1 **Figure 4. Configuration of the metabolite fluxes related to central carbon**
2 **metabolism during early, mid and late exponential growth.** Summary of the
3 metabolite fluxes as predicted by the *i*JN1411 metabolic model constrained by the
4 consumption data indicated in Table S1. The fluxes corresponding to the early
5 exponential phase are indicated in black. Fluxes that change at later times of growth are
6 indicated in red (increased flux) or green (decreased flux). Compounds that are released
7 to the medium and later recycled are indicated in blue. A more detailed distribution of the
8 fluxes is given in Figures S3A (early exponential phase), S4 (mid exponential phase) and
9 S6 (late exponential phase). TCA, tricarboxylic acids cycle; G6P, glucose-6-phosphate;
10 Ac-CoA, acetyl-CoA; PHA, polyhydroxyalkanoates; OAA, oxaloacetate; SUC, succinate;
11 ISO, isocitrate, MAL, malate; CIT, citrate, Pyr, pyruvate, α -KG, α -ketoglutarate.

12
13 **Figure 5. Metabolism of amino acids during early, mid and late exponential growth.**
14 Summary of the fate of the amino acids used as predicted by the *i*JN1411 metabolic
15 model constrained by the consumption data indicated in Table S1. Those used during
16 the early exponential phase are indicated in black. Amino acids for which consumption
17 increased (red) or decreased (green) relative to early exponential growth are highlighted.
18 Those that, after their uptake, are biodegraded within cells are indicated with an asterisk.
19 A more detailed distribution of the fluxes is given in Figures S3B (early exponential
20 phase), S5 (mid exponential phase) and S7 (late exponential phase).

21
22 **Figure 6. Modifications in the configuration of *P. putida* KT2440 metabolism during**
23 **the early, mid and late phases of its exponential growth in LB.** The changes
24 observed in the strategies to obtain energy (reducing power), the TCA configuration, the
25 metabolism of sugars, amino acids and PHAs, as well as in the generation of oxidative
26 stress, are indicated. The representation is merely schematic and by no means
27 quantitative.

28

1 SUPPLEMENTARY MATERIAL

2

3 **Figure S1.** Concentration of free amino acids (black bars) and total amino acids (free +
4 those in polypeptides; grey bars) in LB.

5

6 **Figure S2.** Growth (turbidity at 600 nm) of *P. putida* KT2440 in M9 minimal salts medium
7 with 3 mM glucose (Glc), 5 mM glutamate (Glu), 0.25% of starch, cellobiose, maltodextrin
8 or mannan, or combinations of these polysaccharides with glucose or glutamate.

9

10 **Figure S3.** Predictions of metabolite fluxes for central carbon metabolism (**A**) and amino
11 acid metabolism (**B**) during early exponential growth. The fluxes correspond to those
12 predicted by the *i*JN1411 metabolic model constrained by the consumption data in Table
13 S1. Fluxes >0.1 mmol/g cell dry weight/h are indicated in parentheses. Compounds
14 predicted to be released to the medium are boxed in yellow.

15

16 **Figure S4.** Changes in central carbon metabolism at mid exponential growth compared
17 to early exponential growth according to (**A**) the metabolic flux model, and (**B**) proteomic
18 analysis. Arrows indicate fluxes (A) or proteins (B) that are more abundant (red), or less
19 abundant (green), or do not change (black) with respect to the previous phase. Blue,
20 reactions that do not occur in the initial phase, or that change direction. Arrow thickness
21 is roughly proportional to the fluxes/changes observed. Dashed green lines indicate that
22 some enzymes in the pathway are repressed. Fluxes >0.1 mmol/g cell dry weight/h are
23 indicated in parentheses. Compounds predicted to be extruded are boxed in yellow;
24 those that accumulate are boxed in blue. Reactions inverted (*) or not observed (**)
25 relative to the previous phase are indicated.

26

27 **Figure S5.** Changes in the metabolism of amino acids in mid exponential growth relative
28 to early exponential growth according to (**A**) the metabolic flux model, and (**B**) proteomic

1 analysis. Arrows indicate fluxes (A) or proteins (B) that are more abundant (red), or less
2 abundant (green), or do not change (black), with respect to the previous phase. Arrow
3 thickness is roughly proportional to the fluxes/changes observed. Reactions that do not
4 occur in early exponential growth, or that change direction, are indicated in blue. Dashed
5 green lines indicate that some enzymes in the pathway are repressed. Compounds
6 predicted to be expelled, or accumulated, are boxed in yellow or blue, respectively.
7 Reactions inverted (*) or nor observed (**) relative to the previous phase are indicated.

8

9 **Figure S6.** Changes in central carbon metabolism in late exponential growth relative to
10 mid exponential growth according to (A) the metabolic flux model, and (B) proteomic
11 analysis. Arrows indicate fluxes (A) or proteins (B) that are more abundant (red), or less
12 abundant (green), or do not change (black). Arrow thickness is roughly proportional to
13 the fluxes/changes observed. Reactions that do not occur in mid exponential growth, or
14 that change direction, are indicated in blue. Violet, compounds detected but not included
15 in the model. Dashed lines indicate that some enzymes in the pathway are activated
16 (red) or repressed (green). Compounds predicted to be expelled are boxed in yellow.
17 Compounds predicted to be expelled, or accumulated, are boxed in yellow or blue,
18 respectively. Reactions inverted (*) or nor observed (**) relative to the previous phase
19 are indicated.

20

21 **Figure S7.** Changes in the metabolism of amino acids in late exponential growth relative
22 to mid exponential growth according to (A) the metabolic flux model, and (B) proteomic
23 analysis. Arrows indicate fluxes (A) or proteins (B) that are more abundant (red), or less
24 abundant (green), or do not change (black). Arrow thickness is roughly proportional to
25 the fluxes/changes observed. Reactions that do not occur in mid exponential growth, or
26 that change direction, are indicated in blue. Red dashed lines indicate that some
27 enzymes in the pathway are activated. Compounds predicted to be expelled are boxed

1 in yellow. Reactions inverted (*) or nor observed (**) relative to the previous phase are
2 indicated.

3

4 **Table S1.** Composition of LB before (initial) and after inoculation with *P. putida* KT2440,
5 during early ($A_{600}=0.2$), mid ($A_{600}=0.6$) and late exponential ($A_{600}=2$) growth. The highest
6 consumptions rates for each compound in each growth period are highlighted in grey.
7 The values underlined were determined following predictions made by the flux model.
8 Total glucose refers to free glucose plus that present in polysaccharides. N.d., not
9 determined. (*) Data from reference (La Rosa *et al.*, 2016); (**) TTC reduction assay
10 ($A_{510\text{ nm}}$ ml/mg of cell dry weight).

11

12 **Table S2.** Proteins showing increased or decreased abundance (change ≥ 1.4 fold; \log_2
13 of 0.49), and a q -value of ≤ 0.05 in mid exponential growth relative to early exponential
14 growth (Excel sheet labelled "Mid-vs-Initial"), or in late exponential growth relative to mid
15 exponential growth (Excel sheet labelled "Late-vs-Mid").

16

1 **References**

2

3 Adams, B.L. (2016) The Next Generation of Synthetic Biology Chassis: Moving Synthetic Biology
4 from the Laboratory to the Field. *ACS Synth Biol* **5**: 1328-1330.

5 Aguilar-Uscanga, B., and Francois, J.M. (2003) A study of the yeast cell wall composition and
6 structure in response to growth conditions and mode of cultivation. *Lett Appl Microbiol* **37**:
7 268-274.

8 Bauchop, T., and Eldsen, S.R. (1960) The growth of microorganisms in relation to their energy
9 supply. *J Gen Microbiol* **23**: 457-569.

10 Belda, E., van Heck, R.G., José López-Sánchez, M., Cruveiller, S., Barbe, V., Fraser, C. et al.
11 (2016) The revisited genome of *Pseudomonas putida* KT2440 enlightens its value as a
12 robust metabolic chassis. *Environ Microbiol* **18**: 3403-3424.

13 Chubukov, V., Gerosa, L., Kochanowski, K., and Sauer, U. (2014) Coordination of microbial
14 metabolism. *Nat Rev Microbiol* **12**: 327-340.

15 Crousilles, A., Dolan, S.K., Brear, P., Chirgadze, D.Y., and Welch, M. (2018) Gluconeogenic
16 precursor availability regulates flux through the glyoxylate shunt in *Pseudomonas*
17 *aeruginosa*. *J Biol Chem* **293**: 14260-14269.

18 Defez, R., Andreozzi, A., and Bianco, C. (2017) Quantification of triphenyl-2H-tetrazoliumchloride
19 reduction activity in bacterial cells. *Bio-protocol* **7**: e2115.

20 del Castillo, T., and Ramos, J.L. (2007) Simultaneous catabolite repression between glucose and
21 toluene metabolism in *Pseudomonas putida* is channeled through different signaling
22 pathways. *J Bacteriol* **189**: 6602-6610.

23 del Castillo, T., Ramos, J.L., Rodríguez-Hervá, J.J., Fuhrer, T., Sauer, U., and Duque, E. (2007)
24 Convergent peripheral pathways catalyze initial glucose catabolism in *Pseudomonas putida*:
25 genomic and flux analysis. *J Bacteriol* **189**: 5142-5152.

26 del Castillo, T., Duque, E., and Ramos, J.L. (2008) A set of activators and repressors control
27 peripheral glucose pathways in *Pseudomonas putida* to yield a common central
28 intermediate. *J Bacteriol* **190**: 2331-2339.

29 Dvorak, P., and de Lorenzo, V. (2018) Refactoring the upper sugar metabolism of *Pseudomonas*
30 *putida* for co-utilization of cellobiose, xylose, and glucose. *Metab Eng* **48**: 94-108.

- 1 Ebert, B.E., Kurth, F., Grund, M., Blank, L.M., and Schmid, A. (2011) Response of *Pseudomonas*
2 *putida* KT2440 to increased NADH and ATP demand. *Appl Environ Microbiol* **77**: 6597-6605.
- 3 Escapa, I.F., García, J.L., Buhler, B., Blank, L.M., and Prieto, M.A. (2012) The
4 polyhydroxyalkanoate metabolism controls carbon and energy spillage in *Pseudomonas*
5 *putida*. *Environ Microbiol* **14**: 1049-1063.
- 6 Fedral-Register (1982) Appendix E, Certified host-vector systems. **47**: p. 17197.
- 7 Franklin, F.C., Bagdasarian, M., Bagdasarian, M.M., and Timmis, K.N. (1981) Molecular and
8 functional analysis of the TOL plasmid pWWO from *Pseudomonas putida* and cloning of
9 genes for the entire regulated aromatic ring *meta* cleavage pathway. *Proc Nat Acad Sci USA*
10 **78**: 7458-7462.
- 11 Koul, A., Vranckx, L., Dhar, N., Gohlmann, H.W., Ozdemir, E., Neefs, J.M. et al. (2014) Delayed
12 bactericidal response of *Mycobacterium tuberculosis* to bedaquiline involves remodelling of
13 bacterial metabolism. *Nat Commun* **5**: 3369.
- 14 La Rosa, R., Behrends, V., Williams, H.D., Bundy, J.G., and Rojo, F. (2016) Influence of the Crc
15 regulator on the hierarchical use of carbon sources from a complete medium in
16 *Pseudomonas*. *Environ Microbiol* **18**: 807-818.
- 17 Lanning, M.C., and Cohen, S.S. (1951) The detection and estimation of 2-ketohexonic acids. *J*
18 *Biol Chem* **189**: 109-114.
- 19 López-Serra, P., Marcilla, M., Villanueva, A., Ramos-Fernández, A., Palau, A., Leal, L. et al.
20 (2014) A DERL3-associated defect in the degradation of SLC2A1 mediates the Warburg
21 effect. *Nat Commun* **5**: 3608.
- 22 Matsushita, K., Shinagawa, E., Adachi, O., and Ameyama, M. (1979) Membrane-bound D-
23 gluconate dehydrogenase from *Pseudomonas aeruginosa*. Its kinetic properties and a
24 reconstitution of gluconate oxidase. *J Biochem* **86**: 249-256.
- 25 Molina-Henares, M.A., de la Torre, J., García-Salamanca, A., Molina-Henares, A.J., Herrera,
26 M.C., Ramos, J.L., and Duque, E. (2010) Identification of conditionally essential genes for
27 growth of *Pseudomonas putida* KT2440 on minimal medium through the screening of a
28 genome-wide mutant library. *Environ Microbiol* **12**: 1468-1485.

- 1 Moreno, R., Martínez-Gomariz, M., Yuste, L., Gil, C., and Rojo, F. (2009) The *Pseudomonas*
2 *putida* Crc global regulator controls the hierarchical assimilation of amino acids in a complete
3 medium: evidence from proteomic and genomic analyses. *Proteomics* **9**: 2910-2928.
- 4 Moreno, R., Fonseca, P., and Rojo, F. (2012) Two small RNAs, CrcY and CrcZ, act in concert to
5 sequester the Crc global regulator in *Pseudomonas putida*, modulating catabolite repression.
6 *Mol Microbiol* **83**: 24-40.
- 7 Moreno, R., Hernández-Arranz, S., La Rosa, R., Yuste, L., Madhushani, A., Shingler, V., and
8 Rojo, F. (2015) The Crc and Hfq proteins of *Pseudomonas putida* cooperate in catabolite
9 repression and formation of ribonucleic acid complexes with specific target motifs. *Environ*
10 *Microbiol* **17**: 105-118.
- 11 Nelson, K.E., Weinel, C., Paulsen, I.T., Dodson, R.J., Hilbert, H., Martins dos Santos, V.A. et al.
12 (2002) Complete genome sequence and comparative analysis of the metabolically versatile
13 *Pseudomonas putida* KT2440. *Environ Microbiol* **4**: 799-808.
- 14 Nikel, P.I., Martínez-García, E., and de Lorenzo, V. (2014) Biotechnological domestication of
15 pseudomonads using synthetic biology. *Nat Rev Microbiol* **12**: 368-379.
- 16 Nikel, P.I., Chavarria, M., Fuhrer, T., Sauer, U., and de Lorenzo, V. (2015) *Pseudomonas putida*
17 KT2440 Strain Metabolizes Glucose through a Cycle Formed by Enzymes of the Entner-
18 Doudoroff, Embden-Meyerhof-Parnas, and Pentose Phosphate Pathways. *J Biol Chem* **290**:
19 25920-25932.
- 20 Nogales, J., Palsson, B.O., and Thiele, I. (2008) A genome-scale metabolic reconstruction of
21 *Pseudomonas putida* KT2440: *iJN746* as a cell factory. *BMC Syst Biol* **2**: 79.
- 22 Nogales, J., Gudmundsson, S., Duque, E., Ramos, J.L., and Palsson, B.O. (2017) Expanding
23 The Computable Reactome In *Pseudomonas putida* Reveals Metabolic Cycles Providing
24 Robustness. *bioRxiv* **139121**, <https://doi.org/10.1101/139121>.
- 25 Oh, Y.K., Palsson, B.O., Park, S.M., Schilling, C.H., and Mahadevan, R. (2007) Genome-scale
26 reconstruction of metabolic network in *Bacillus subtilis* based on high-throughput
27 phenotyping and gene essentiality data. *J Biol Chem* **282**: 28791-28799.
- 28 Orth, J.D., Thiele, I., and Palsson, B.O. (2010) What is flux balance analysis? *Nat Biotechnol* **28**:
29 245-248.

- 1 Plata, M.R., Koch, C., Wechselberger, P., Herwig, C., and Lendl, B. (2013) Determination of
2 carbohydrates present in *Saccharomyces cerevisiae* using mid-infrared spectroscopy and
3 partial least squares regression. *Anal Bioanal Chem* **405**: 8241-8250.
- 4 Poblete-Castro, I., Becker, J., Dohnt, K., Dos Santos, V.M., and Wittmann, C. (2012) Industrial
5 biotechnology of *Pseudomonas putida* and related species. *Appl Microbiol Biotechnol* **93**:
6 2279-2290.
- 7 Puchalka, J., Oberhardt, M.A., Godinho, M., Bielecka, A., Regenhardt, D., Timmis, K.N. et al.
8 (2008) Genome-scale reconstruction and analysis of the *Pseudomonas putida* KT2440
9 metabolic network facilitates applications in biotechnology. *PLoS Computational Biology* **4**:
10 e1000210.
- 11 Ramos-Fernández, A., Paradelo, A., Navajas, R., and Albar, J.P. (2008) Generalized method for
12 probability-based peptide and protein identification from tandem mass spectrometry data
13 and sequence database searching. *Mol Cell Proteomics* **7**: 1748-1754.
- 14 Rojo, F. (2010) Carbon catabolite repression in *Pseudomonas*: optimizing metabolic versatility
15 and interactions with the environment. *FEMS Microbiol Rev* **34**: 658-684.
- 16 Sambrook, J., and Russell, D.W. (2001) *Molecular cloning: a laboratory manual*. Cold Spring
17 Harbor, N.Y.: Cold Spring Harbor Laboratory.
- 18 Sawyer, M.H., Baumann, P., Baumann, L., Berman, S.M., Canovas, J.L., and Berman, R.H.
19 (1977) Pathways of D-fructose catabolism in species of *Pseudomonas*. *Arch Microbiol* **112**:
20 49-55.
- 21 Schellenberger, J., Que, R., Fleming, R.M., Thiele, I., Orth, J.D., Feist, A.M. et al. (2011)
22 Quantitative prediction of cellular metabolism with constraint-based models: the COBRA
23 Toolbox v2.0. *Nat Protoc* **6**: 1290-1307.
- 24 Sezonov, G., Joseleau-Petit, D., and D'Ari, R. (2007) *Escherichia coli* physiology in Luria-Bertani
25 broth. *J Bacteriol* **189**: 8746-8749.
- 26 Sonnleitner, E., Abdou, L., and Haas, D. (2009) Small RNA as global regulator of carbon
27 catabolite repression in *Pseudomonas aeruginosa*. *Proc Natl Acad Sci USA* **106**: 21866-
28 21871.
- 29 Sonnleitner, E., Wulf, A., Campagne, S., Pei, X.Y., Wolfinger, M.T., Forlani, G. et al. (2018)
30 Interplay between the catabolite repression control protein Crc, Hfq and RNA in Hfq-

- 1 dependent translational regulation in *Pseudomonas aeruginosa*. *Nucleic Acids Res* **46**:
2 1470-1485.
- 3 van Schie, B.J., Hellingwerf, K.J., van Dijken, J.P., Elferink, M.G., van Dijk, J.M., Kuenen, J.G.,
4 and Konings, W.N. (1985) Energy transduction by electron transfer via a pyrrolo-quinoline
5 quinone-dependent glucose dehydrogenase in *Escherichia coli*, *Pseudomonas aeruginosa*,
6 and *Acinetobacter calcoaceticus* (var. *Iwoffii*). *J Bacteriol* **163**: 493-499.
- 7 Varma, A., and Palsson, B.O. (1995) Parametric sensitivity of stoichiometric flux balance models
8 applied to wild-type *Escherichia coli* metabolism. *Biotechnol Bioeng* **45**: 69-79.
- 9 Ward Jr, J.H. (1963) Hierarchical Grouping to Optimize an Objective Function. *J Am Stat Assoc*
10 **58**: 236-244.
- 11 Wessel, D., and Flugge, U.I. (1984) A method for the quantitative recovery of protein in dilute
12 solution in the presence of detergents and lipids. *Anal Biochem* **138**: 141-143.
- 13 Wittgens, A., Tiso, T., Arndt, T.T., Wenk, P., Hemmerich, J., Müller, C. *et al.* (2011) Growth
14 independent rhamnolipid production from glucose using the non-pathogenic *Pseudomonas*
15 *putida* KT2440. *Microb Cell Fact* **10**: 80.
- 16
17

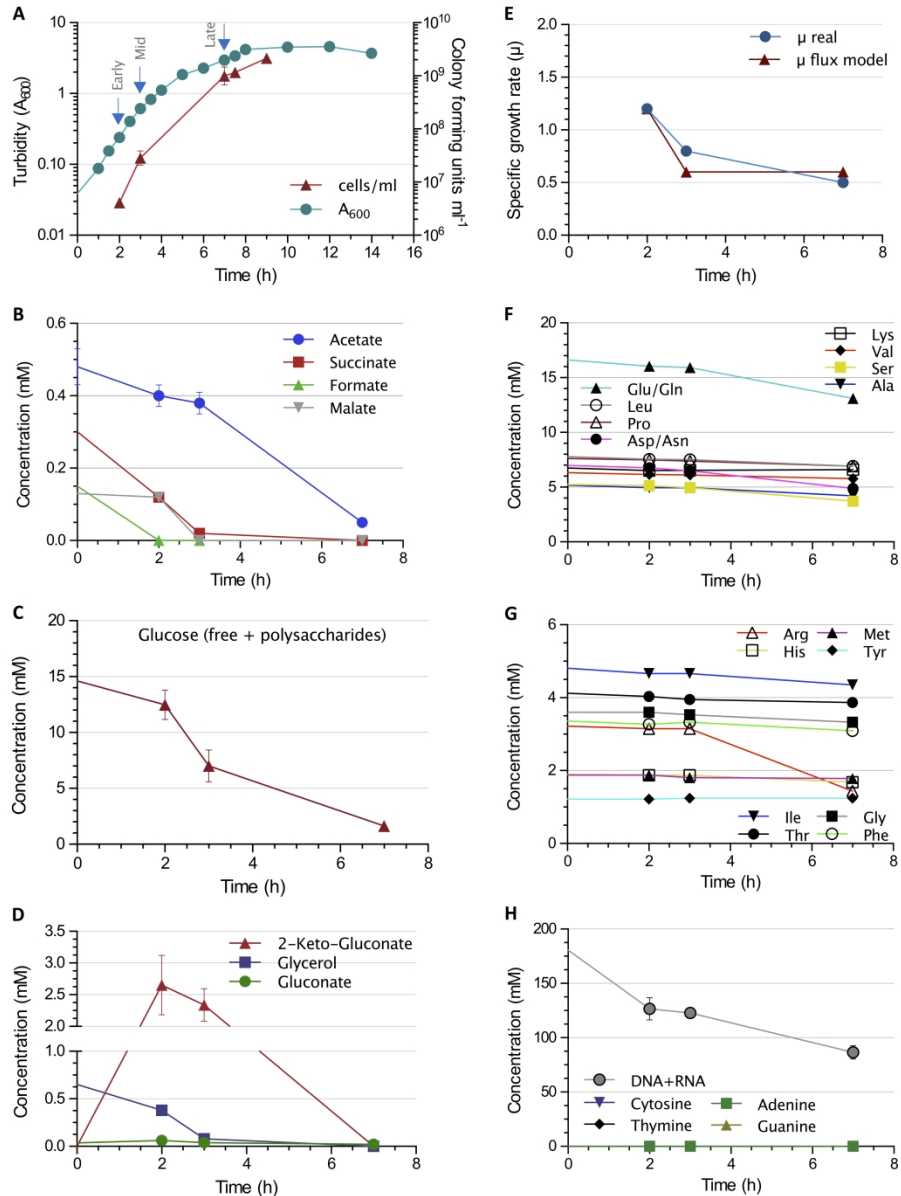


Figure 1. Growth of *P. putida* KT2440 in LB and consumption of different compounds. (A) Increase in turbidity (A_{600}) and in colony forming units (cells/ml) during growth in LB. Consumption of organic acids (B), sugars (glucose monomers and polymers) (C), amino acids (F, G) and (poly) nucleotides (H) during growth. (D) Release of 2-ketogluconate and gluconate to the medium and consumption of glycerol during growth. (E) Growth rate at each time point relative to the previous point (or to the inoculated cells in the case of the first time point); data derived either from the experimentally determined increase in biomass (μ real), or from the increase predicted by the flux model (μ flux model). Error bars indicate the standard deviation of three independent assays. The scale of the time axis is not the same in all panels.

153x204mm (600 x 600 DPI)

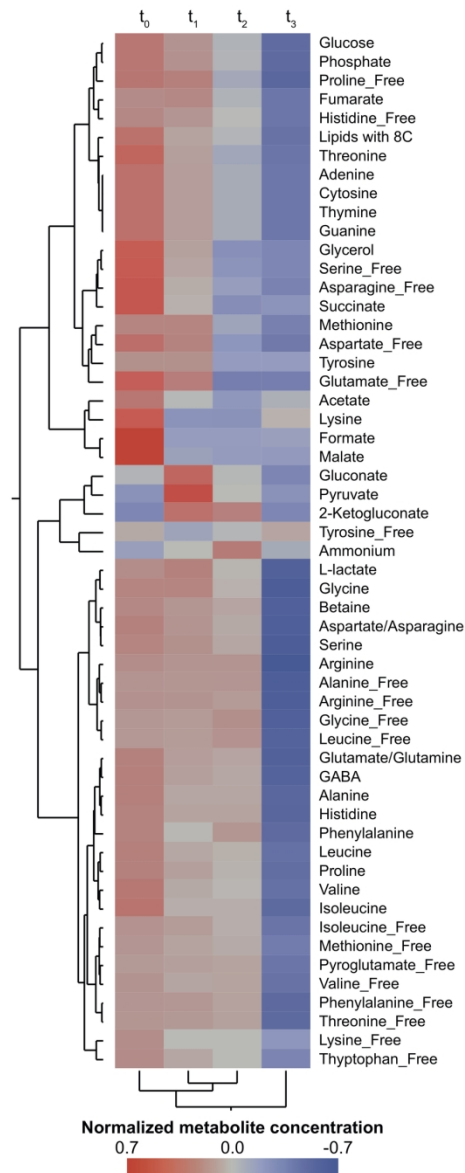


Figure 2. Hierarchical clustering of the exo-metabolomic profiles of *P. putida*. The normalised concentrations (range scaling) of each metabolite identified in the non-inoculated medium (t_0), or in medium samples collected at the early (t_1), mid (t_2) and late (t_3) exponential phases of growth (data derived from Table S1), were clustered according to Euclidean distances using the Ward clustering algorithm (Ward Jr, 1963) and employing JMP software v.13.2. The highest normalised concentration for each compound is indicated in red colour, while the lowest concentration is in blue.

86x206mm (300 x 300 DPI)

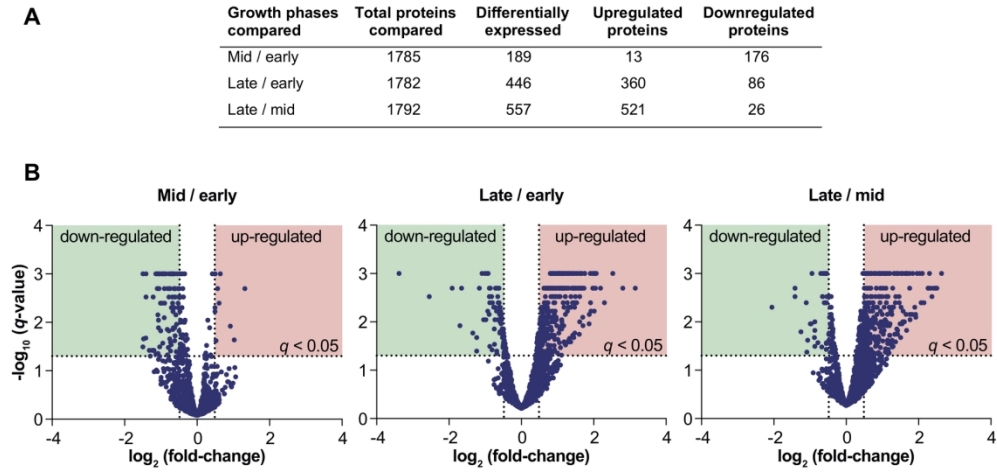


Figure 3. Comparison of the proteome of cells collected at early, mid and late exponential growth. (A) Number of proteins detected and compared under each condition, and those differentially expressed (q -value <0.05 , fold-change >1.4 , as recommended (Koul et al., 2014)). (B) Volcano plots of the proteins showing increased or decreased abundance during early, mid and late exponential growth. Differentially expressed proteins are listed in Table S2 (Supplementary Material).

165x79mm (300 x 300 DPI)

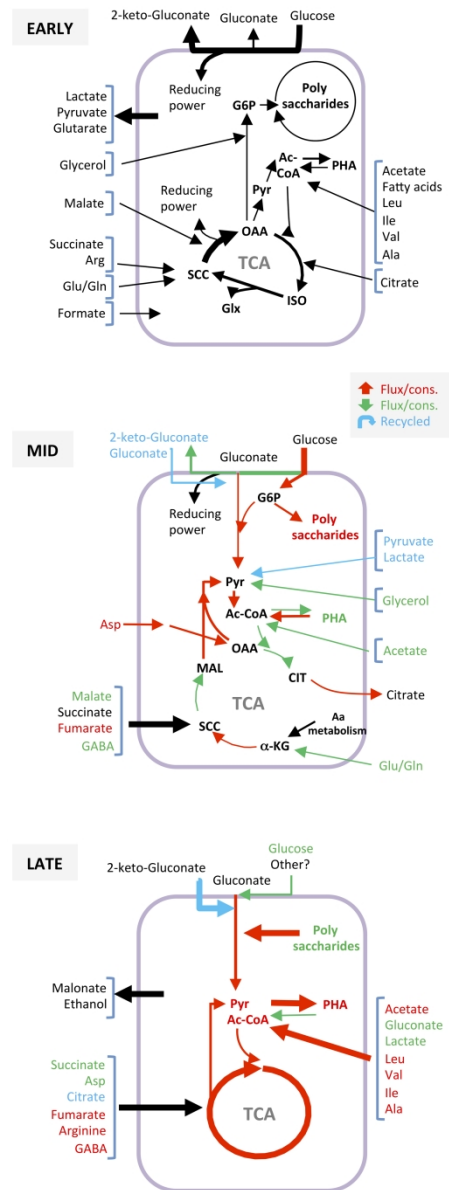


Figure 4. Configuration of the metabolite fluxes related to central carbon metabolism during early, mid and late exponential growth. Summary of the metabolite fluxes as predicted by the iJN1411 metabolic model constrained by the consumption data indicated in Table S1. The fluxes corresponding to the early exponential phase are indicated in black. Fluxes that change at later times of growth are indicated in red (increased flux) or green (decreased flux). Compounds that are released to the medium and later recycled are indicated in blue. A more detailed distribution of the fluxes is given in Figures S3A (early exponential phase), S4 (mid exponential phase) and S6 (late exponential phase). TCA, tricarboxylic acids cycle; G6P, glucose-6-phosphate; Ac-CoA, acetyl-CoA; PHA, polyhydroxyalkanoates; OAA, oxaloacetate; SUC, succinate; ISO, isocitrate, MAL, malate; CIT, citrate, Pyr, pyruvate, α -KG, α -ketoglutarate.

80x212mm (600 x 600 DPI)

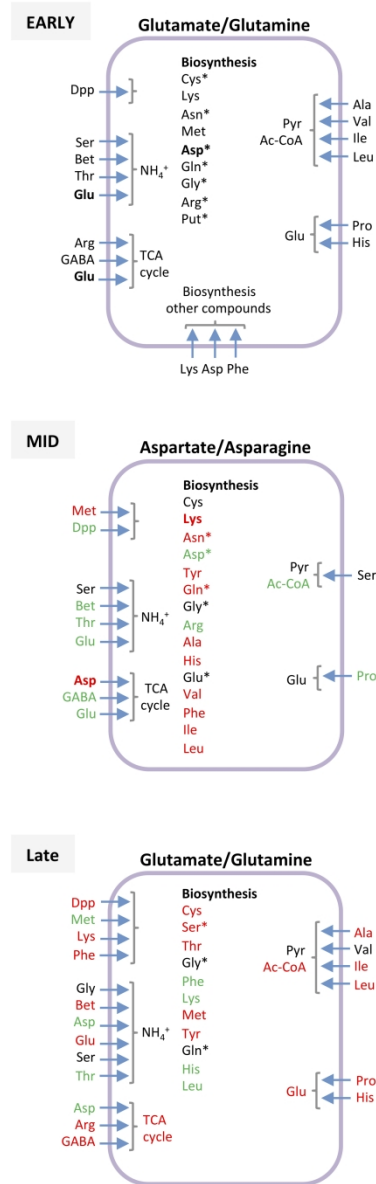


Figure 5. Metabolism of amino acids during early, mid and late exponential growth. Summary of the fate of the amino acids used as predicted by the iJN1411 metabolic model constrained by the consumption data indicated in Table S1. Those used during the early exponential phase are indicated in black. Amino acids for which consumption increased (red) or decreased (green) relative to early exponential growth are highlighted. Those that, after their uptake, are biodegraded within cells are indicated with an asterisk. A more detailed distribution of the fluxes is given in Figures S3B (early exponential phase), S5 (mid exponential phase) and S7 (late exponential phase).

64x202mm (600 x 600 DPI)

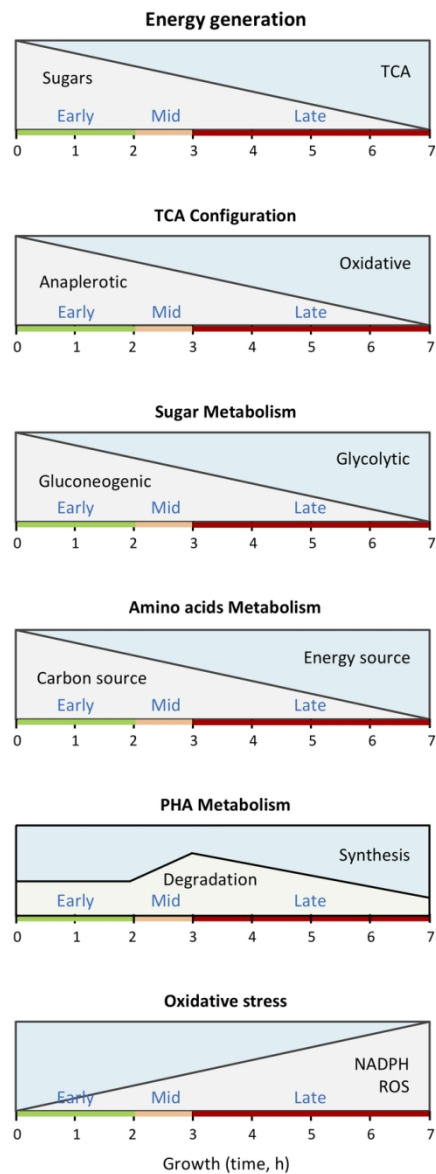


Figure 6. Modifications in the configuration of *P. putida* KT2440 metabolism during the early, mid and late phases of its exponential growth in LB. The changes observed in the strategies to obtain energy (reducing power), the TCA configuration, the metabolism of sugars, amino acids and PHAs, as well as in the generation of oxidative stress, are indicated. The representation is merely schematic and by no means quantitative.

57x158mm (300 x 300 DPI)